International Journal of Machine Tools & Manufacture 50 (2010) 901–910

Contents lists available at ScienceDirect

International Journal of Machine Tools & Manufacture

journal homepage: www.elsevier.com/locate/ijmactool

Grinding–hardening using dry air and liquid nitrogen: Prediction and verification of temperature fields and hardened layer thickness

Thai Nguyen *, L.C. Zhang

School of Mechanical and Manufacturing Engineering, The University of New South Wales, NSW 2052, Australia

ARTICLE INFO

Article history:
Received 22 March 2010
Received in revised form
31 May 2010
Accepted 4 June 2010
Available online 15 June 2010

Keywords:
Grinding–hardening
Temperature field
Liquid nitrogen
3D finite element analysis
Heat treatment

ABSTRACT

This paper investigates the grinding–hardening both theoretically and experimentally with a plunge surface-grinding process. Theoretically, the paper presents a temperature-dependent finite element heat transfer model, incorporating a triangular moving heat source and various cooling conditions, to investigate the phase transformation kinetics, thus to predict the thickness of a layer hardened. The temperature variation and thickness of the hardened layer were also investigated experimentally on quenchable steel 1045 using dry air and liquid nitrogen as the cooling media. The predictions were in good agreement with the experimental results. It was found that the phase transformation follows the martensitic kinetics. The application of liquid nitrogen enhances the transformation of retained austenite to martensite and results in a refinement of the martensitic structure.

1. Introduction

It is important that machine components subjected to frequent contact sliding have hardened surfaces of high wear resistance while maintaining their toughness for the sake of the durability of the components. In the current manufacturing practice, to achieve such requirement, it has to follow an ineffective process which is costly, consumes energy and is not efficient. Workpieces after a soft machining need to be transported to the surface hardening bay, cleaned and heat treated. They are then discharged, moved back and incorporated into the production line of grinding for a final precision surface finish. Such a production procedure is clearly not cost-effective, involves serious occupational and health problems associated with the use of toxic coolants [1], and is not technically desirable as it wastes most grinding energy and makes it difficult to protect the treated surface microstructure.

Grinding–hardening is a technology that uses the heat generated in grinding to create a hardened surface layer by promoting the phase transformation in ground quenchable steel components [2–4]. Metallurgical studies on the layer hardened by this method have shown an enhancement of dislocation and carbon distribution compared to that of conventional quenching, and such microstructural alterations resulted in a remarkable improvement in wear and fatigue resistances [5,6]. Moreover, in conjunction with the application of liquid nitrogen, it was found that compressive residual stresses, a beneficial property that guards against most stress-induced failures of a machine component, were developed within the martensitic structure, and that a ground surface could be prevented from oxidisation [7]. These results promise a feasible solution for integrating grinding and the heat treatment into a single process of grinding–hardening, producing components with superior surface integrity.

The kinetics of phase transformations in steel depends greatly on the temperature and time during a heat treatment process [8–10]. Unlike conventional heat treatment methods where the heating and quenching cycles can be relatively easily controlled, thermal cycle in grinding is a complex process. The grinding heat source, approximately triangular [11–13] is generated within a small wheel–workpiece contact area. While this heat source is moving along a workpiece, the material in the heat source vicinity experiences convective cooling. Such a transient heat transfer process can result in a variation in thickness and microstructure of the grinding-hardened layer. Experimental methods developed so far to measure the temperature have been limited either by the destructive way (e.g. PVD film method [14] and thermocouple sensors [15]) or by the restriction of the visible zone (e.g. CCD camera [13] or infrared), which are not suitable for a grinding process where the heating zone is interfered by the condensed moisture as in the application of cooling media. The heat transfer analysis of grinding to date is limited to two-dimensional cases. There is no investigation on the grinding–hardening under cryogenic conditions.

The present study will first establish a temperature-dependent, three-dimensional (3D) heat transfer model based on the

* Corresponding author. Tel: +61 2 9385 5689.
E-mail addresses: thai.nguyen@unsw.edu.au, thai.h.nguyen@gmail.com (T. Nguyen), Liangchi.Zhang@unsw.edu.au (L.C. Zhang).

0890-6955/$ - see front matter
doi:10.1016/j.ijmachtools.2010.06.002

Nomenclature

A_0	average single grain–workpiece contact area, m^2
b, n	kinetic parameters in Eq. (A4.1)
B	width ground, m
C_p	specific heat, J kg^{-1} K^{-1}
C_{jk}, D_{jk}	polynomial coefficients in Eq. (A4.2)
D	wheel diameter, m
d	wheel depth of cut, m
d_g	wheel grain size, m
$f(\xi)$	correction function, Eq. (A2.2)
F_t	tangential component of grinding force, N
G_a	number of active grains per unit area of the wheel surface
H	thickness of the sample, m
h_a	heat transfer coefficient due to air flow, W m^{-2} K^{-1}
h_b	heat transfer coefficient due to boiling, W m^{-2} K^{-1}
k	thermal conductivity of workpiece, W m^{-1} K^{-1}
k_a	thermal conductivity of air, W m^{-1} K^{-1}
L	workpiece length, m
l_c	wheel–workpiece contact length, m
M	manufacturing grit number
Nu	Nusselt number
$\vec{n}$	vector normal to the surface of a boundary, m
Re	Reynolds number
Pr	Prandtl number
$\dot{q}$	heat rate per unit volume, W m^{-3}
q_c	heat flux due to convection, W m^{-2}
q_r	heat flux due to radiation, W m^{-2}
$\overline{q}_g$	average grinding heat flux, W m^{-2}
$q_g(\chi)$	grinding heat flux function over the contact length, W m^{-2}
q_0	peak on a triangle grinding heat flux profile, W m^{-1}
t	time, s
t_0	time for a heat source to move over the distance of a unit length and a, sec
t_l	time for a heat source to move over the distances of a contact length, s
T	temperature, K or °C
T_f	film temperature (T_f=0.5(T_w+T_∞)), K or °C
T_w	wall temperature, K or °C
T_{sat}	saturated temperature, K or °C
T_∞	ambient temperature, K or °C
ΔT_{sat}	boiling temperature difference ($\Delta T = T_w - T_{sat}$), K or °C
Δt_k	duration of the time step at temperature T_k, s
ΔH_i	enthalpy of transformation, J kg^{-1}
f_i	volume fraction of phase i
v_s	wheel speed, m s^{-1}
v_w	table (heat source) speed, m s^{-1}
V_p	volumetric packaging density of grains in the wheel constituent
x, y, z	coordinate components of the system
α	thermal diffusivity ($\alpha = k/\rho C_p$), $m^2 s^{-1}$
ε	emissivity
χ, ζ, ψ	coordinate components of the moving heat source
η	partition of energy contributed into the workpiece
τ^*	fictitious time, s
τ_k	time for the beginning of isothermal transformation at temperature T_k
υ	air viscosity, m^2 s^{-1}
ρ	workpiece density, kgm^{-3}
σ	Stefan–Boltzmann constant (σ=5.67 × 10^{-8} W m^{-2} K^{-4})

finite element method to predict the temperature field during the processes and the consequent thickness of hardened layer in grinding–hardening. Experimentation will then be carried out to verify the theoretical prediction.

2. Mathematical Modelling

2.1. Thermal analysis

Fig. 1 illustrates the schematic diagram of thermal conduction in surface grinding. The calculation of temperature field is based on an unsteady-state heat conduction equation [16]

$$\frac{\partial}{\partial x}\left(k\frac{\partial T}{\partial x}\right)+\frac{\partial}{\partial y}\left(k\frac{\partial T}{\partial y}\right)+\frac{\partial}{\partial z}\left(k\frac{\partial T}{\partial z}\right)+\dot{q}=\frac{1}{\alpha}\frac{\partial T}{\partial t} \quad (1)$$

where $\dot{q}$ is the heat rate per unit volume generated during phase transformation, k the thermal conductivity, $\alpha = k/\rho C_p$ the thermal diffusivity in which ρ is the density and C_p the specific heat.

During phase transformation, there is an associated change in enthalpy. In the quenching process, the microstructure of the steel is assumed to be a mixture of austenite, ferrite, pearlite, bainite and martensite. The linear law of mixture is adopted through which $\dot{q}$ can be derived as [8]

$$\dot{q}=\frac{\rho}{\Delta t}\sum_{i=2}^{5}\frac{\partial \Delta H_i}{\partial f_i}df_i \quad (2)$$

where f_i is the volume percentage of phase i, ΔH_i the enthalpy of transformation, taken as 75.2, 92.0, 92.0 and 83.6 kJkg^{-1} for the austenite→ferrite, austenite→pearlite, austenite→bainite and austenite→martensite reactions, respectively.

The thermal properties (k, ρ and C_p) of the workpiece material are temperature-dependent (shown in Appendix 1), which are accommodated in the finite element computation using ANSYS. Eq. (1) was solved subject to the initial and boundary conditions as described below:

2.1.1. Initial conditions

$T_\infty = 22$°C (constant ambient temperature), (3)

$$T(x,y,z,t)\big|_{t=0}=T_\infty,\quad 0\le x\le L,\quad 0\le y\le B,\quad -H\le z\le 0 \quad (4)$$

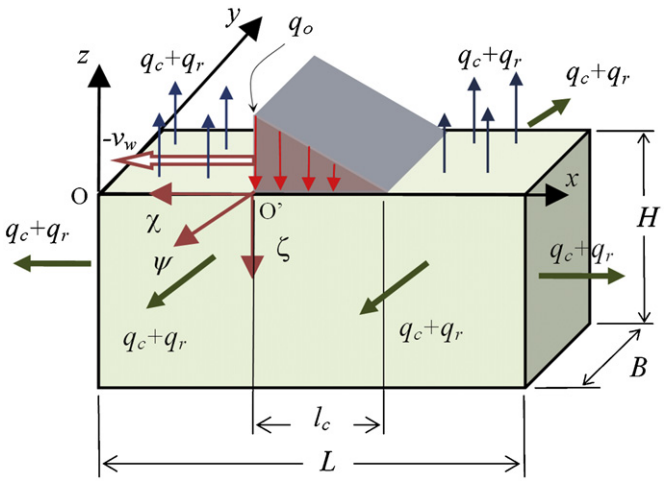

Fig. 1. Diagram of the moving heat source model.

2.1.2. Boundary condition for heating—moving heat source

The surface heat flux due to grinding, q_g, can be viewed as a moving heat source on a moving coordinate system, χ–ζ–ψ, at a constant speed, $-v_w$, along a workpiece surface with a fixed coordinate system, x–y–z. In plunge grinding, a heat source has a constant width in the ψ-direction, which is the same as that of a workpiece, B, as illustrated in Fig. 1. For up grinding, the distribution of the heat flux is triangular, having a linear distribution over a wheel–workpiece contact length, l_c, and can be expressed as

$$q_g(\chi)|_{t=const} = q_0 - \frac{q_0}{l_c}|\chi|, \quad 0 \geq \chi \geq -l_c \tag{5}$$

where q_0 is the peak heat flux that can be obtained from the experiment, i.e.,

$$q_0 = \frac{2}{l_c}\int_0^{-l_c} q(\chi)d\chi = 2\bar{q}_g \tag{6}$$

in which, according to [17,18],

$$\bar{q}_g = \eta\frac{F_t v_s}{Bl_c} \tag{7}$$

where $\bar{q}_g$ is the average grinding heat flux, η is the fraction of total energy conducted as heat into the workpiece (heat partition ratio) that can be determined according to the analysis of burn prediction (Appendix 2), v_s is the wheel speed, F_t is the tangential component of grinding force and $l_c = \sqrt{Dd}$ [17] in which D is the wheel diameter and d is the wheel depth of cut.

2.1.3. Neumann boundary conditions for cooling

$$-k\frac{\partial T}{\partial \vec{n}} = q_c + q_r = h(T_w - T_\infty) + \varepsilon\sigma(T_w^4 - T_\infty^4) \tag{8}$$

where $\vec{n}$ is the unit vector normal to the surface of a boundary, q_c and q_r are the surface heat fluxes associated with the convective cooling and radiation, respectively, h is the heat transfer coefficient applied to the boundary surface, T_w is the wall surface temperature [16], σ is the Stefan–Boltzmann constant and ε is the material's emissivity (ε=0.21 [16]).

The convective heat transfer coefficient applied to the surface normal to $\vec{n}_x$ and $\vec{n}_y$ is

$$h|_{z<0} = h_a \tag{9}$$

where h_a is the heat transfer coefficient due to air flow, determined in Appendix A3.1.

However, on the top surface of the workpiece where the grinding heat flux is applied, there is only the area outside the grinding zone subjected to convective cooling [19]. Depending on the cooling applications, the heat transfer coefficient is determined as follows:

- For the dry air application,

$$h|_{z=0} = \begin{cases} 0, & 0 \geq \chi \geq -l_c \quad \text{(within the grinding zone)} \\ h_a, & \chi < -l_c, \chi > 0 \quad \text{(outside the grinding zone)} \end{cases} \tag{10}$$

- For the application of liquid nitrogen, due to the limit of liquid nitrogen penetration into the grinding zones [7], there is only the region afterward the grinding zone subjected to the liquid nitrogen, i.e.,

$$h|_{z=0} = \begin{cases} h_a, & \chi > 0 \quad \text{(frontward the grinding zone)} \\ 0, & 0 \geq \chi \geq -l_c \quad \text{(within the grinding zone)} \\ h_b, & \chi < -l_c, \chi > 0 \quad \text{(afterward the grinding zone)} \end{cases} \tag{11}$$

where h_b is the heat transfer coefficient due to boiling of liquid nitrogen ejected from a nozzle, determined in Appendix A3.2.

Radiation is also applicable for the boundary surface exposed to the ambient, i.e.,

$$q_r = \begin{cases} 0, & 0 \geq \chi|_{z=0} \geq -l_c \\ \varepsilon\sigma(T_w^4 - T_\infty^4), & (\chi|_{z=0} < -l_c, \chi|_{z=0} > 0) \cup z < 0 \end{cases} \tag{12}$$

2.2. Prediction of hardened layer thickness

In a grinding–hardening process, the development of a hardened layer is the result of phase transformations, where the steel is heated to a temperature above the Ac3 temperature at which the completion of the transformation corresponds to a full austenitic structure [20]. By probing the peak temperature developed at the Ac3 at a subsurface distance in the component subjected to grinding, the thickness of the hardened layer at an instant location can be determined [17,18].

Microstructure evolution of a heat treated component after undergoing the Ac3 is determined by the kinetics of phase transformation. Based on the continuous cooling transformation (CCT) diagram (Fig. 2), the kinetics of phase transformation depends on the cooling rate. The phase transformation can be divided into two groups: diffusion controlled transformations and martensitic transformation.

The kinetics of diffusional transformations (decomposition of austenite to pearlite, ferrite or bainite) is predicted following a procedure outlined by Refs. [8,20–22] (Appendix 4)

$$f_k = 1 - \exp[-b(\Delta t + \tau^*)^n] \tag{13}$$

where f_k is the volume fraction of the constituents (k=1 for ferrite/pearlite and k=2 for bainite), b and n are the kinetic parameters obtained from isothermal measurements, shown in Appendix 4, τ^* is the fictitious time transformation time for each time step Δt, i.e.,

$$\tau^* = \left[\frac{\ln(1-f_m)}{-bT_{m+1}}\right]^{1/nT_{m+1}}. \tag{14}$$

The martensitic transformation is considered not to be time-dependent. Below the M_s temperature, transformation starts independently of the cooling rate [21]. The rate of transformation for the austenite-to-martensite reaction is calculated from the empirical equation proposed by Koistinen and Marburger [23]

$$f_M = 1 - \exp[-\gamma(M_s - T_q)] \tag{15}$$

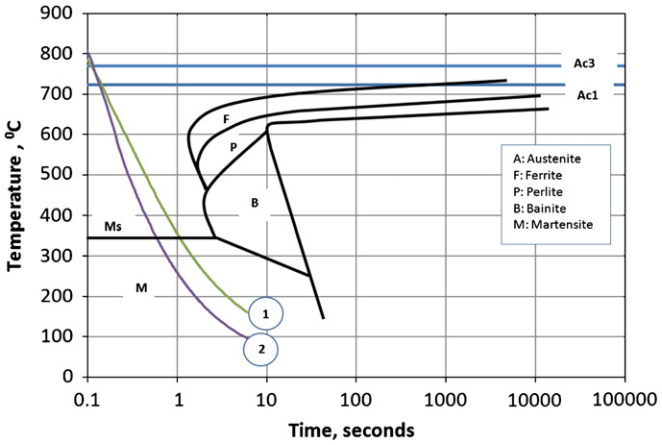

Fig. 2. CCT diagram of 1045 steel (after Ref. [37]). Cooling curves for (1) dry air application and (2) liquid nitrogen application.

where γ is a constant, which was found to be 0.011 for most steels and T_q the quenching temperature.

The increment of fraction transformed is used to calculate the heat released, $\dot{q}$ which is then incorporated in Eq. (1).

3. Experiment

Fig. 3 illustrates the experimental setup. The tests were conducted on 1045 steel using a surface-grinding machine, Minini Junior 90CF CNC M286. The experimental setup for the application of liquid nitrogen was detailed elsewhere [7]. Liquid nitrogen was ejected at 50 kPa from a 2 mm diameter nozzle placed at a distance of 50 mm and an angle of 30° tangential to the workpiece surface (Fig. 3b). After grinding, a ground workpiece was left in liquid nitrogen for 600 s, and then increased to the ambient temperature. To avoid moisture from air, because if it is trapped inside a liquid nitrogen reservoir it can cause an explosive reaction, the internal pressure of the reservoir was maintained by feeding from a compressed nitrogen gas vessel. Grinding conditions are listed in Table 1.

Table 1
Experimental conditions.

Grinding method	• Surface up grinding • Dressing: single point diamond, traverse rate = 160 μm/rev with total dressing depth = 5 μm × 25 μm
Sample	• 1045 steel • Dimension (mm) ($L \times W \times D$) = 60 × 15 × 20
Grinding wheel	• 57A60LV (alumina) ∅300 mm × 27 mm • Thermal properties at 300 K [36]: k (W m^{-1} K^{-1}) = 46, ρ (kg m^{-3}) = 3970, C_p (J kg^{-1} K^{-1}) = 770
Wheel speed (m/s)	25
Table speed (mm/min)	1000
Depth of cut (μm)	50 and 100
Cooling	• Atmospheric dry air, ambient temperature = 25 °C • Liquid nitrogen: jet injection with flow rate of 36.3 cc/s

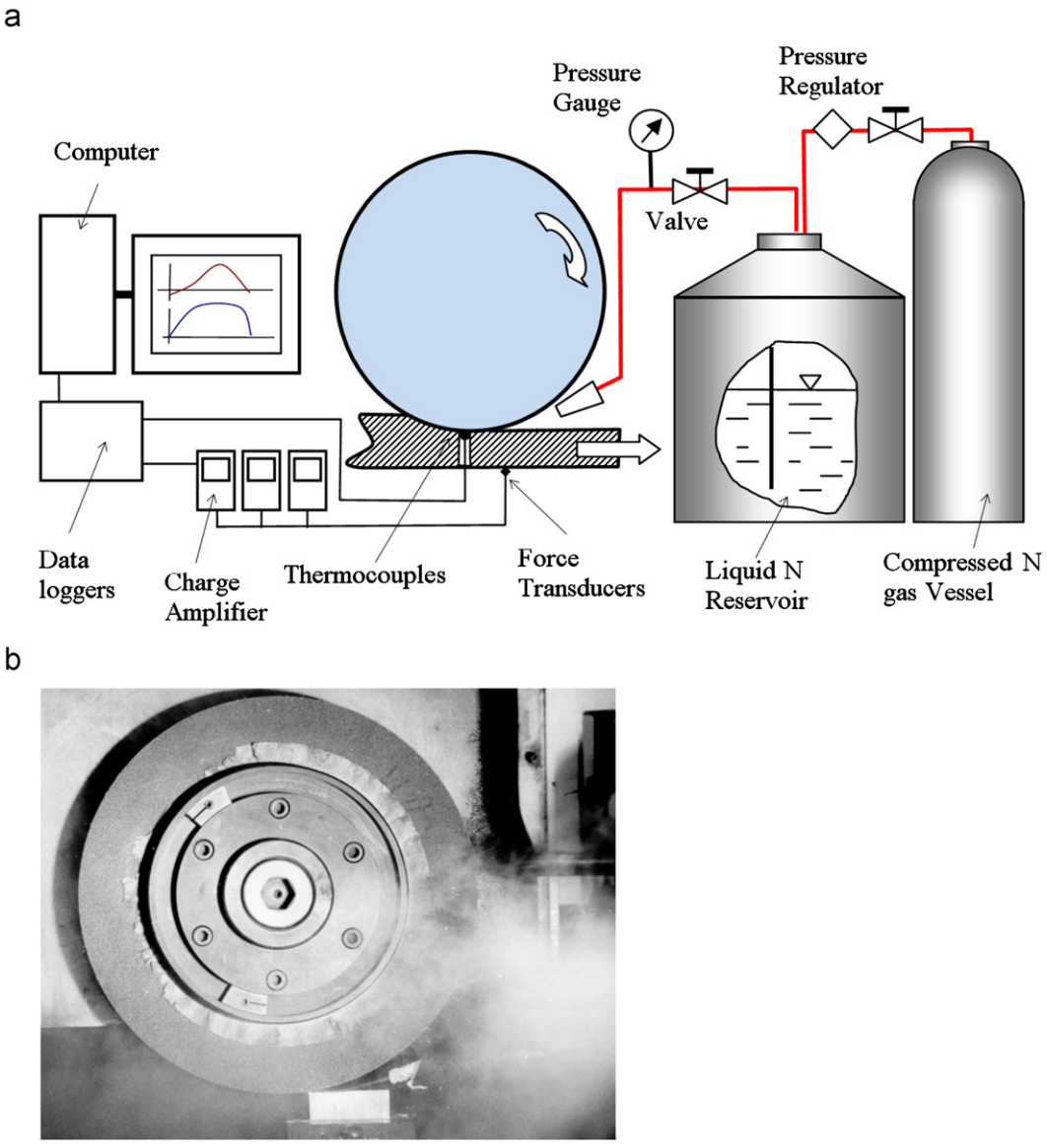

Fig. 3. Experimental setup. (a) Diagram of experimental setup. (b) Liquid nitrogen application.

Grinding forces in the directions along and traverse with the workpiece were measured using a Kistler 9257B dynamometer. Temperature history during grinding was detected using a thermocouple technique. Type K-thermocouple wires were guided inside the specimen to the surface to be ground where their junctions were embedded. To minimise thermal lag, a response time required for a thermocouple approaching the temperature of measured media [24], small thermocouple wires of 0.0125 mm diameter were used. The wires were metal-shielded to eliminate the signal noise. To cope with rapid temperature fluctuation (typically 0.1–1 s) in grinding, a data acquisition (DAQ) system equipped with a high frequency response DAQ board, NI SCXI-1600 (sampling rate of 200 kS/s), a signal conditioning module, SCXI-1102B (high bandwidth of 200 Hz) and an isothermal terminal block, SCXI-1303 was used. The data were collected and analysed using the *Labview* (*Laboratory Virtual Instrumentation Workbench*) program.

4. Results and discussion

The predictions of peak temperature are listed in Table 2, showing an agreement with the measurements where the discrepancy of the peak values is in the range of −7.8% to −12.9%. Hardened layers were only created at a higher depth of cut (100 μm) where the grinding heat was sufficient for raising the workpiece to above the austenite temperature Ac3. Fig. 4a and b show the prediction of temperature responses in grinding at the depth of cut 100 μm with dry air and liquid nitrogen, respectively. It shows that the use of liquid nitrogen does not significantly reduce the peak temperature in the grinding zone. This is because, as revealed experimentally [7], the penetration of liquid nitrogen into the grinding zone is extremely limited such that the high heat dissipation due to the boiling of liquid nitrogen is effective only outside the grinding zone. The cooling conditions were accounted in the model as represented by Eqs. (11) and (12). The model verified by experimental results (Fig. 4b) confirms that grinding–hardening can be achieved under the application of liquid nitrogen.

Fig. 5a and b show the temperature fields in grinding with dry air and liquid nitrogen, respectively. Due to the heat transfer on the sides of the block, isothermal lines are in the parabola form with the highest temperature occurring at the adiabatic plane at the middle of the block. The front of the component ground with liquid nitrogen shows a distinct feature of the "tail" of the isothermal lines. At a certain distance from the surface, temperature is higher than that at the surface. This is because the high heat transfer rate of liquid nitrogen makes the top surface under the liquid nitrogen jet experiencing a higher cooling rate. This occurs until at a distance in the subsurface at which the heat flow rate to the upper surface and that to the bottom of the ground component reaches a balance.

By probing the peak temperature developed at the Ac3 (795 °C for the 1045 steel) at subsurface distances of the ground components, thickness of the hardened layers can be determined [17,18]. Before a workpiece can engage with the grinding wheel with a full contact length (l_c=5.4 mm), the heat generated is small that results in a hardened layer with the thickness varying along the grinding direction, x, as shown in Fig. 6a and b. In the region where $x \geq 5.4$ mm, the hardened thickness can be considered uniformly. The predictions of hardened thickness layer in this stable region agree well with the experimental results (Fig. 6c and d) within 4.2% and 7.4% for grinding under dry air and liquid nitrogen, respectively, as shown in Table 2. It is noticed that the hardened layer thickness generated by the application of liquid nitrogen is smaller than that by applying dry air. This is because the cooling rate in the workpiece subsurface (via conduction) at the application of liquid nitrogen is much higher so that

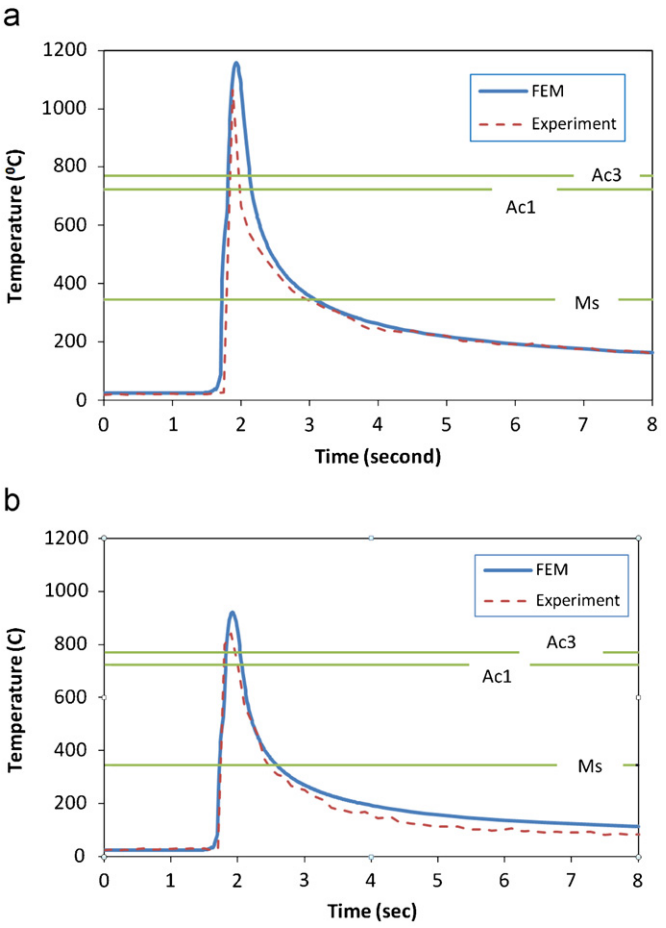

Fig. 4. Temperature response in grinding–hardening using different cooling media: (4a) under dry air, and (4b) with liquid nitrogen.

Table 2
Experimental results.

Cooling media	Depth of cut (μm)	Peak temperature (°C)			Hardened thickness [a] (μm)		
		Prediction	Measurement	Discrepancy (%)	Prediction	Measurement	Discrepancy (%)
Dry Air	50	743	658	−12.9	Nil	Nil	N/A
	100	1158	1064.5	−8.8	596	622	4.2
Liquid nitrogen	50	484	432	−12.0	Nil	Nil	N/A
	100	908	842	−7.8	280	302	7.4

[a] At the stable region, middle of the ground components.

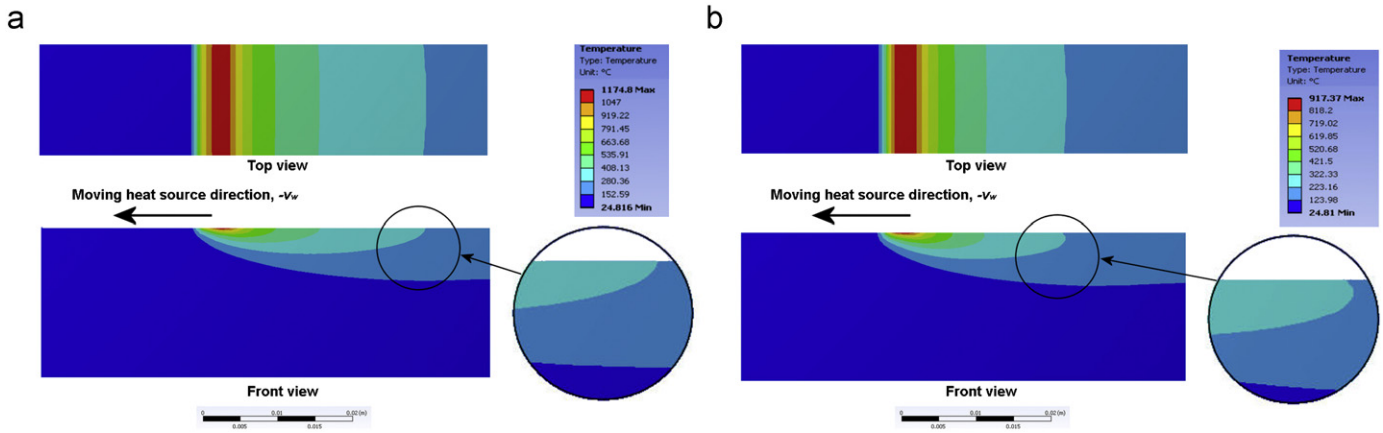

Fig. 5. Temperature fields developed in grinding–hardening using different cooling media: (5a) under dry air, and (5b) with liquid nitrogen.

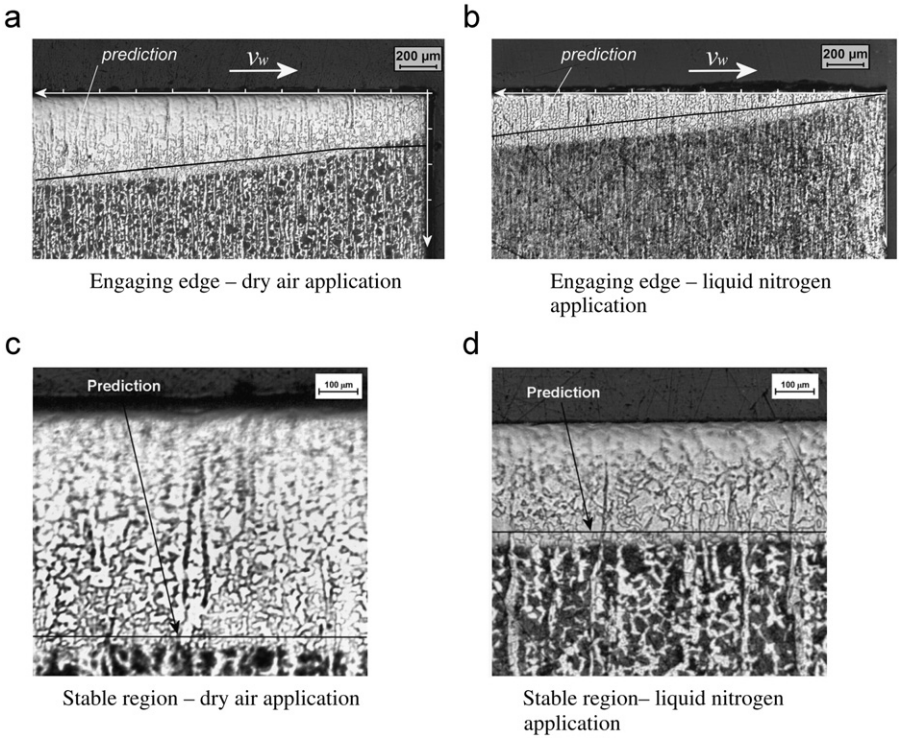

Fig. 6. Hardened layers developed at (6a and 6b) the engaging edges of the ground components and at (6c and 6d) stable region of the ground components using different cooling media: (6a and 6c) under dry air and (6b and 6d) with liquid nitrogen.

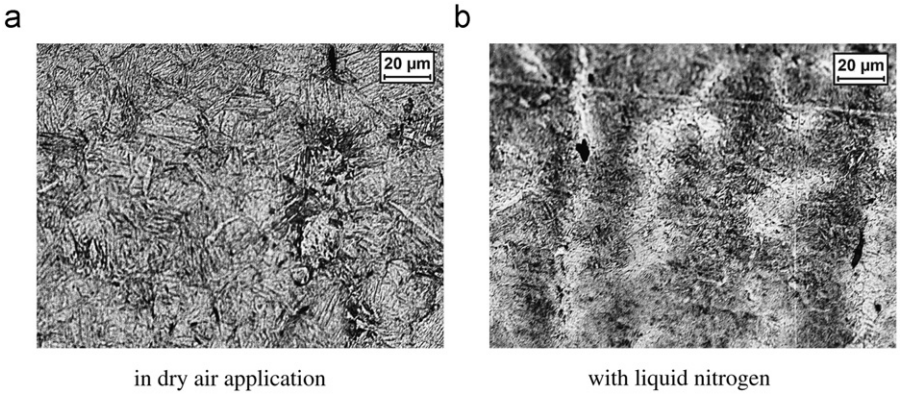

Fig. 7. Martensitic microstructure of the layer hardened by grinding–hardening with different cooling media (observed on the top ground surface)

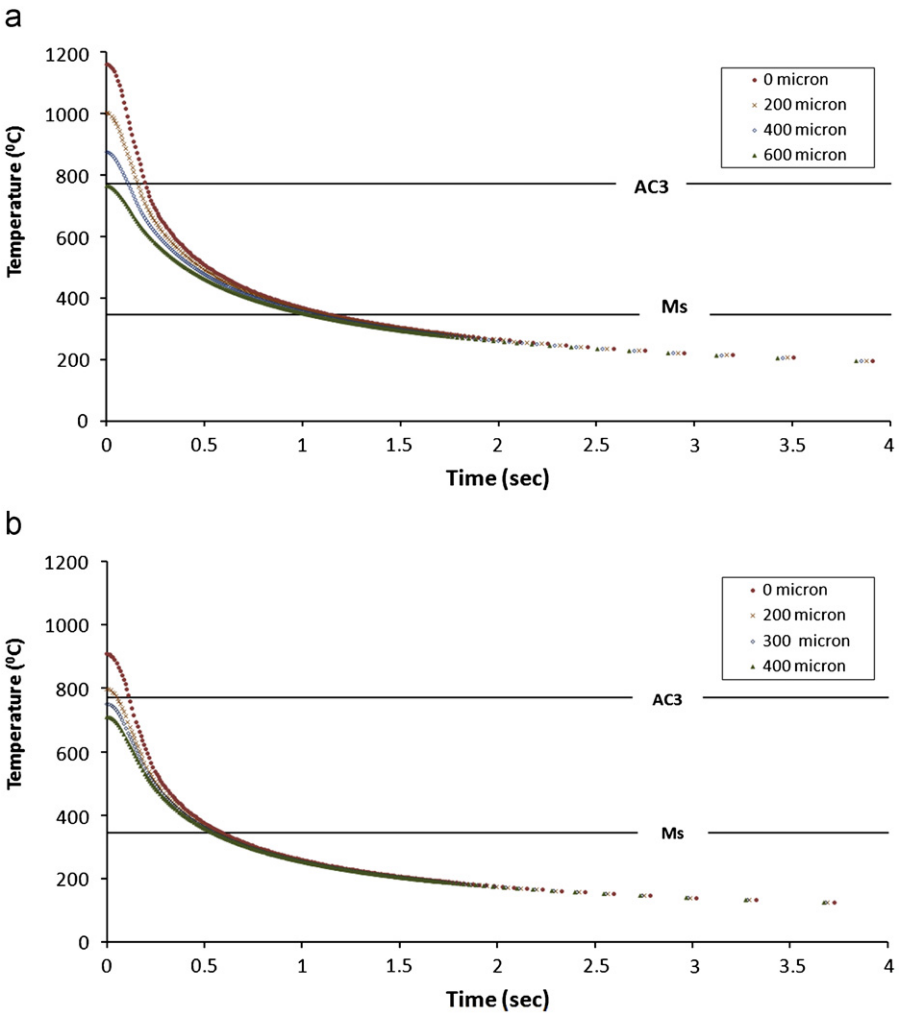

Fig. 8. Cooling curves detected at the middle of components and at different subsurface distances subject to grinding (a) with dry air, and (b) with liquid nitrogen

the thickness of the material that can experience the phase transformation is smaller.

Fig. 7 shows the microstructures of the hardened layers in grinding generated by the applications of dry air and liquid nitrogen. Martensitic laths were found within the hardened layers. The details of microstructural analysis and associated mechanical property changes can be found in the works conducted by the authors and co-workers [5,7]. This was due to the transformation kinetics associated with the cooling history. Fig. 8 shows the cooling curves detected at the middle of hardened components and at different subsurface distances. When the table speed was high (100 mm/min), the new austenite layers formed by the heat generated within the grinding zone were rapidly exposed to the cooling media. The high cooling rates allowed the cooling curves to pass through the M_s (within approximate 0.5 and 1.0 s for the dry air and liquid nitrogen applications, respectively), by-passing the ferrite, pearlite and bainite regions (Fig. 2). The phase change from austenite to martensite in both the cooling applications was not diffusion controlled but driven by the martensitic kinetics.

The martensitic formation occurs in both the cases of cooling applications. However, the layer hardened by grinding with liquid nitrogen constitutes with finer martensite structure (Fig. 7b). In the martensitic kinetics, as stated in Eq. (15), the amount of martensite formed is related to the undercooling below the M_s. Effects of liquid nitrogen in grinding–hardening is to continue the transformation of retained austenite to martensite [7,25].

5. Conclusion

A temperature-dependent heat transfer model incorporating the moving heat source, based on the finite-element method, has been developed to predict the temperature field and consequent hardened thickness in the grinding of a 3D block. The model was applied to grinding–hardening under dry air and liquid nitrogen cooling conditions. The prediction and experimental results agreed well for steel 1045.

The phase transformation followed the martensitic kinetics. Effects of liquid nitrogen in grinding–hardening is to continue the transformation of retained austenite to martensite that resulted in a refinement of martensitic structure.

The model provides a fundamental insight into the heat transfer mechanism in grinding–hardening, which can be used for the process optimisation.

Acknowledgement

This project was financially supported by the Australian Research Council (ARC).

Appendices

A1. Thermal and mechanical properties of workpiece

The thermal and mechanical property data for 1045 steel [8,26] are shown in Fig. 9.

A2. Heat partition ratio

The heat partition ratio (η) can be determined according to the analysis of burn prediction [27]

$$\eta = \left\{1 + 1.06\left[\frac{(k\rho C_p)_s v_s}{(k\rho C_p)_w v_w}\right]^{0.5} f(\xi) A_0 G_a\right\}^{-1} \tag{A2.1}$$

where the function $f(\xi)$ takes into account the fact that the wheel grain cross-section area is substantially higher than the contact area between the wheel grain and the workpiece and is given as [15]

$$f(\xi) = \frac{2}{\pi^{0.5}} \frac{\xi}{1 - \exp(\xi^2)\mathrm{erf}(\xi)} \tag{A2.2}$$

$$\xi = \left(\frac{\gamma \pi \alpha_s l_c}{2 A_0 v_s}\right)^{0.5} \tag{A2.3}$$

In Eqs. (A2.1–A2.3), the subscripts s and w denote wheel grain and workpiece, respectively, γ is an abrasive shape factor, taken to be unit since grains used in making the grinding wheels are approximately equiaxed [28], ($\alpha = k/\rho C_p$) is the thermal diffusivity, A_0 the average single grain–workpiece contact area corresponding to the truncated of the cone and G_a the number of active grains per unit area of the wheel surface.

The thermal properties of the wheel at 300 K are shown in Table 1 [29].

The average single grain–workpiece contact area A_0 can be approximated as 5% of the projected grain area ($\pi d_g^4/4$) [15] where the grain size (d_g) is computed as [18]

$$d_g(\mathrm{mm}) = 64 M^{-1.4} \tag{A2.4}$$

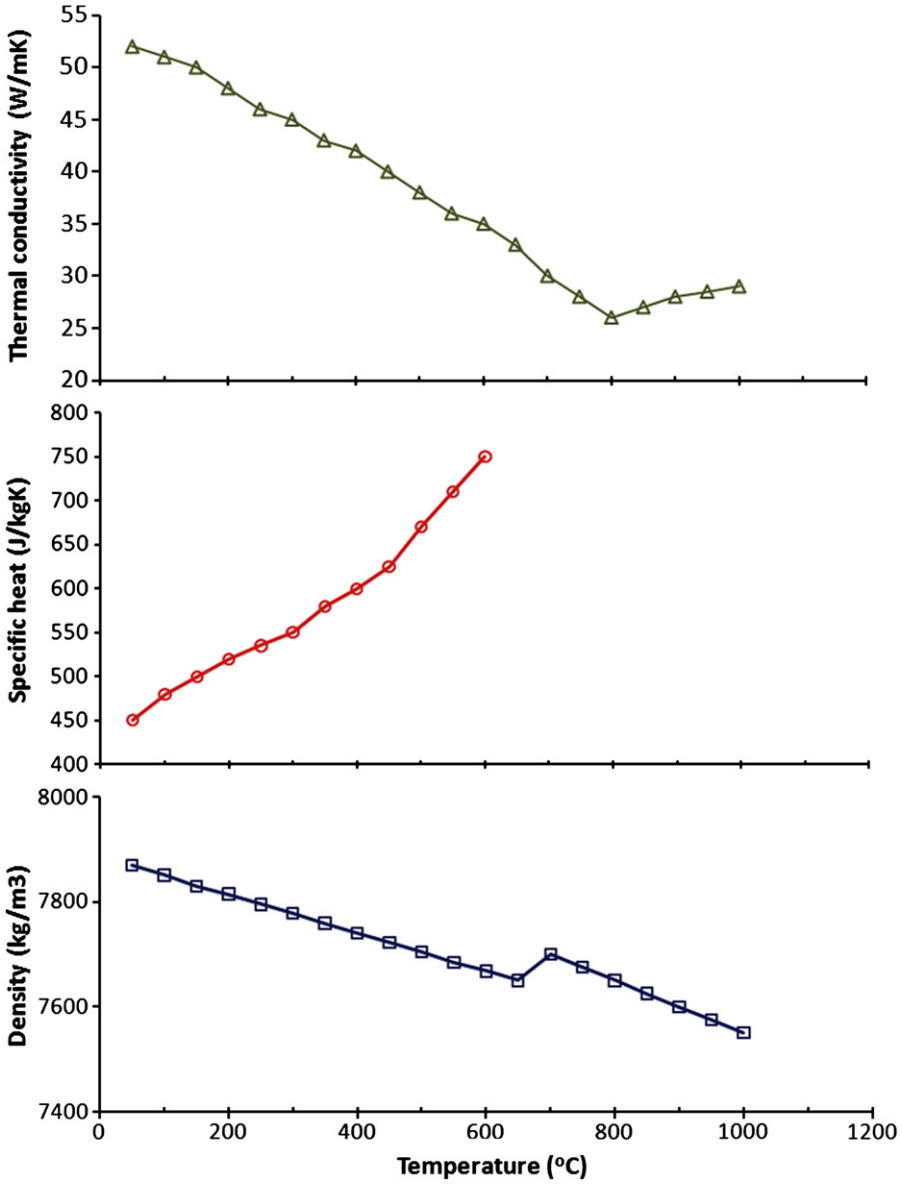

Fig. 9. Thermo-mechanical properties of the sample, steel 1045 [8].

where M is the manufacturing grit number ($M=60$ for the wheel used in this study).

The number of active grains per unit area of the wheel surface (G_a) is calculated by

$$G_a = \frac{1}{(\pi d_g^4/4)V_p} \tag{A2.5}$$

where V_p is the volumetric packaging density of grains in the wheel constituent, taken as 40% for the aluminium oxide wheel [30].

For the experimental setup given in Table 1, the heat partition ratio calculated is in the range of 57–68%. These values are in agreement with other works [15].

A3. Heat transfer coefficient

A3.1. Grinding in dry air

The heat transfer coefficient, h_a, is estimated following the empirical correlation for a square section with a characteristic length (B) subject to a cross flow of air [16,31]

$$Nu = \frac{h_a B}{k_a} = 0.102 Re^{0.675} Pr^{1/3} \tag{A3.1}$$

where Nu, Pr and Re are the Nusselt, Prandtl and Reynolds numbers, respectively. The flow of air is induced by the relative motion of the wheel and the workpiece, thus Re can be defined as

$$Re = \frac{(v_s \pm v_w)B}{\upsilon} \approx \frac{v_s B}{\upsilon} \tag{A3.2}$$

where υ is the viscosity of air; the sign of $\pm$ is associated with the up and down grindings, respectively.

Since $v_s \gg v_w$,

$$Re \approx \frac{v_s B}{\upsilon}. \tag{A3.3}$$

The thermal properties of air (k_a, υ and Pr) are functions of temperature and are considered at the film temperature, $T_f=0.5(T_w+T_\infty)$. For the given grinding conditions in Table 1, the dependency of heat transfer coefficient on the wall surface temperature within the range 22–1495 °C which is the melting temperature of workpiece material, is computed as

$$h_a = 485.4(T_w+T_\infty)^{-0.359} \tag{A3.4}$$

where h_a is in W/m^2 K, T_w and T_∞ are in °C and $T_\infty=22$°C (initial condition).

A3.2. Grinding with liquid nitrogen

Due to the cryogenic nature, upon the interaction of liquid nitrogen jets with a metal surface, boiling occurs. Film boiling, which has very low heat transfer coefficient due to radiation from vapour blanket, can exist when the wall temperature is higher than a critical value. This particularly occurs upon the impact of liquid nitrogen on a ground surface which has just experienced a temperature rise from the grinding zone. Much higher convective heat transfer due to the nucleated boiling can be obtained within a lower range of wall temperature. This happens during the quenching process of grinding–hardening. Data from the experiments conducted by [32,33] for a liquid nitrogen jets vertically impacting on a steel surface are adapted in the present study. Correlation between the heat transfer coefficient, h_b, and the superheat temperature ($\Delta T_{sat}=T_w-T_{sat}$) is reproduced and represented as shown

$$h_b = \begin{cases} 91.2\Delta T_{sat}{}^{1.03}, & 68 \geq \Delta T_{sat} > 10 \text{ (nucleate boiling)} \\ -117.1\Delta T_{sat} + 14480, & 118 > \Delta T_{sat} > 68 \text{ (transition boiling)} \\ 1900, & \Delta T_{sat} \geq 118 \text{ (film boiling)} \end{cases} \tag{A3.5}$$

where h_b is in W/m^2 K, $T_{sat}=-196$ °C is the boiling temperature of liquid nitrogen at atmospheric pressure and T_w is in °C.

A4. Kinetic parameters in equations of diffusion transformations

The kinetics of isothermal diffusion transformation are derived by Johnson and Mehl [34] in the Avrami-type equation:

$$f_k = 1-\exp(-bt^n) \tag{A4.1}$$

where f_k is the volume fraction of the constituents ($k=1$ for ferrite/pearlite and $k=2$ for bainite), b and n are the kinetic parameters obtained from isothermal measurements, which according to the Ref. [35] can be approximated by polynomial, i.e.,

$$\log b = C_{0k}+C_{1k}T+C_{2k}T^2+C_{3k}T^3,$$
$$n = D_{0k}+D_{1k}T+D_{2k}T^2+D_{3k}T^3. \tag{A4.2}$$

where log is the base 10 logarithm.

Constants C_{jk} and D_{jk} are determined by the time–temperature-transformation (TTT) diagram of 1045 steel and the minimum quadrate method, listed in Table 3.

However, for the continuous cooling such as in grinding, Scheil's principle is used to estimate the incubation period for the diffusion transformation. The TTT is discretised into a series of isothermal steps. On each step, the volume fraction of new phase formed is calculated using isothermal kinetics. Transformation starts when

$$\sum_k \frac{\Delta t_k}{\tau_k} = 1 \tag{A4.3}$$

where Δt_k denotes the duration of the time step at temperature T_k, τ_k is the time for the beginning of isothermal transformation at temperature T_k.

The transformation is calculated along isotherms and isochors. The time reduces to a fictitious time, τ^* that represents the time needed to transform the actual amount f_m at the end of the time step. The transformation time, t_i, i.e., the time elapsed from the beginning of the diffusion transformation, is obtained as

$$t_i = \Delta t + \tau^* \tag{A4.4}$$

where

$$\tau^* = \left[\frac{\ln(1-f_m)}{-bT_{m+1}}\right]^{1/nT_{m+1}}. \tag{A4.5}$$

Table 3
Constants in Eq. (A4.2).

	C_{0k}	C_{1k}	C_{2k}	C_{3k}
$k=1$	-0.328×10^{2}	0.152	−0.02348	1.200×10^{6}
$k=2$	−6.358	0.01854	0.222×10^{-4}	0
	D_{0k}	D_{1k}	D_{2k}	D_{3k}
$k=1$	0.147×10^{-2}	−6.256	0.9245×10^{-3}	-0.4691×10^{-6}
$k=2$	−21.93	0.1102	-0.1216×10^{-3}	0

Eq. (A4.1) becomes

$$f_k = 1-\exp[-b(\Delta t+\tau^*)^n]. \quad \text{(A4.6)}$$

References

[1] J. Bardin, E.A. Eisen, S.R. Woskie, R.R. Monson, T.J. Smith, P. Tolbert, K. Hanmond, M. Hallock, Mortality studies of machining fluid exposure in the automobile industry: a case-control study of pancreatic cancer, American Journal of Industrial Medicine 32 (1997) 240–247.

[2] L. Zhang, Grinding–hardening of steel surfaces: a focus review, International journal of abrasive technology 1 (1) (2007) 3–36.

[3] E. Brinksmeier, T. Brockhoff, Utilization of grinding heat as a new heat treatment process, CIRP Annals—Manufacturing Technology 45 (1) (1996) 283–286.

[4] T. Brockhoff, E. Brinksmeier, Grind-hardening: a comprehensive view, CIRP Annals—Manufacturing Technology 48 (1) (1999) 255–260.

[5] I. Zarudi, L.C. Zhang, Mechanical property improvement of quenchable steel by grinding, Journal of Materials Science 37 (18) (2002) 3935–3943.

[6] I. Zarudi, L.C. Zhang, Modelling the structure changes in quenchable steel subjected to grinding, Journal of Materials Science 37 (20) (2002) 4333–4341.

[7] T. Nguyen, I. Zarudi, L.C. Zhang, Grinding–hardening with liquid nitrogen: mechanisms and technology, International Journal of Machine Tools and Manufacture 47 (1) (2007) 97–106.

[8] Y. Nagasaka, J.K. Brimacombe, E.B. Hawbolt, I.V. Samarasekera, B. Hernandez-Morales, S.E. Chidiac, Mathematical model of phase transformations and elastoplastic stress in the water spray quenching of steel bars, Metallurgical Transactions A 24A (1993) 795–808.

[9] H. Bhadeshia, in: Bainite in Steels—Transformations, Microstructure and Properties., 2nd ed., The University Press, Cambridge, 2001.

[10] T. Inoue, S. Nagaki, T. Kishino, M. Monkawa1, Description of transformation kinetics, heat conduction and elastic–plastic stress in the course of quenching and tempering of some steels, Archive of Applied Mechanics (Ingenieur Archiv) 50 (5) (1981) 315–327.

[11] L.C. Zhang, T. Suto, H. Noguchi, T. Waida, An overview of applied mechanics in grinding, Manufacturing Review 5 (4) (1992) 261–273.

[12] L.C. Zhang, T. Suto, H. Noguchi, T. Waida, Applied mechanics in grinding, Part III: a new formula for contact length prediction and a comparison of available models, International Journal of Machine Tools and Manufacture 33 (4) (1993) 587–597.

[13] I. Zarudi, L.C. Zhang, A revisit to some wheel–workpiece interaction problems in surface grinding, International Journal of Machine Tools and Manufacture 42 (8) (2002) 905–913.

[14] T. Kato, H. Fujii, Temperature measurement of workpiece in surface grinding by PVD film method, Journal of Manufacturing Science and Engineering, Transactions of the ASME 119 (4(B)) (1997) 689–694.

[15] S. Kohli, C. Guo, S. Malkin, Energy partition to the workpiece for grinding with aluminium oxide and CBN abrasive wheels, Transactions of the ASME 117 (1995) 160–168.

[16] F.P. Incropera, D.P. Dewitt, in: Fundamentals of Heat and Mass Transfer, 3rd ed., John Wiley & Sons Inc., 1990.

[17] M.C. Shaw, in: Principles of Abrasive Processing, Oxford University Press, 1996.

[18] S. Malkin, in: Grinding Technology—Theory and Applications of Machining with Abrasives, Ellis Horwood Ltd., 1989.

[19] M. Mahdi, L.C. Zhang, Applied mechanics in grinding, Part V: thermal residual stresses, International Journal of Machine Tools and Manufacture 37 (5) (1997) 619–633.

[20] S. Denis, D. Farias, A. Simon, Mathematical model coupling phase transformations and temperature evolutions in steels, ISIJ International 32 (3) (1992) 316–325.

[21] J. Rohde, A. Jeppsson, Literature review of heat treatment simulations with respect to phase tranformation, residual stresses and distortion, Scandinavian Journal of Metallurgy 29 (2000) 47–62.

[22] C. Verdi, A. Visintin, A mathematical model of the austenite-pearlite transformation in plain carbon steel based on the Scheil's additivity rule, Acta Metallurgica 35 (11) (1987) 2711–2717.

[23] D.P. Koistinen, R.E. Marburger, A general equation prescribing the extent of the austenite–martensite transformation in pure iron–carbon alloys and plain carbon steels, Acta Metallurgica 7 (1) (1959) 59–60.

[24] J.W. Dally, W.F. Riley, K.G. McConnell, in: Instrumentation for Engineering Measurements, 2nd ed., John Wiley & Sons, Inc., 1993.

[25] P. Gorden, M. Cohen, The transformation of retained austenite in high speed steel at subatmospheric temperatures, Transactions of American Society for Metals 30 (1942) 569–591.

[26] E. Griffiths, Physical constants of some commercial steels at elevated temperatures, The British Iron and Steel Research Association, Butterworths Scientific Publication, London, 1953.

[27] C. Guo, S. Malkin, Heat transfer in grinding, Journal of Materials Processing and Manufacturing Science 1 (1) (1992) 16–27.

[28] C. Guo, Y. Wu, V. Varghese, S. Malkin, Temperatures and energy partition for grinding with vitrified CBN wheels, Annals of the CIRP 48 (1) (1999) 247–250.

[29] A.S. Lavine, A simple model for convective heat transfer during the grinding process, Journal of Engineering for Industry 110 (1988) 1–6.

[30] S. Malkin, C. Guo, in: Grinding Technology: theory and Application of Machining with Abrasives, 2nd ed., Industrial Press, NewYork, 2008.

[31] M. Jakob, Heat Transfer, vol. 1, Wiley, New York, 1949.

[32] G.A. Dreitser, Heat transfer enhancement in channels for film boiling of cryogenic liquids, Applied Thermal Engineering 25 (16) (2005) 2512–2521.

[33] A. Sakurai, M. Shiotsu, K. Hata, Boiling heat transfer characteristics for heat inputs with various increasing rates in liquid nitrogen, Cryogenics 32 (5) (1992) 421–429.

[34] W.A. Johnson, R.F. Mehl, Reaction Kinetics in Processes of Nucleation and Growth, Trans. AIME 135 (1939) 416–458.

[35] C. Heming, H. Xieqing, W. Honggang, Calculation of the residual stress of a 45 steel cylinder with a non-linear surface heat-transfer coefficient including phase transformation during quenching, Journal of Materials Processing Technology 89-90 (1999) 339–343.

[36] A.S. Lavine, T.C. Jen, Coupled heat transfer to workpiece, wheel, and fluid in grinding, and the occurence of workpiece burn, International Journal of Heat and Mass Transfer 34 (4/5) (1991) 983–992.

[37] G.E. Totten, M.A.H. Howes, T. Inoue, in: Handbook of residual stress and deformation of steel, ASM International, 2002.